Drift-Diffusion Modeling for Impurity Photovoltaic Devices

Albert S. Lin and Jamie D. Phillips, *Senior Member, IEEE*

***Abstract*—A 1-D drift-diffusion modeling for impurity photovoltaics is presented. The model is based on the self-consistent solution of Poisson's equation and carrier continuity equations incorporating generation and recombination mechanisms including the intermediate states. The model is applied to a prototypical solar cell device, where strong space charge effects and reduced conversion efficiency are identified for the case of lightly doped absorption regions. A doping compensation scheme is proposed to mitigate the space charge effects, with optimal doping corresponding to one-half the concentration of the intermediate states. The compensated doping device design provides calculated conversion efficiencies of approximately 40%, which is similar to the maximum expected values from prior 0-D models. The carrier transport between intermediate levels is shown to be noncritical for achieving the efficiency limit predicted by 0-D models. The qualitative behavior of the model is compared to existing experimental data on quantum dot solar cells.**

***Index Terms*—Drift-diffusion model, intermediate levels (ILs), semiconductor, solar cell.**

I. Introduction

SOLAR cells based on materials with multiple absorption transitions present an alternative technology to multijunction cells in order to exceed the Shockley and Queisser limit. In this approach, a narrow band of electron states is inserted into the absorption region of the semiconductor to provide additional optical transition paths. These optical transitions provide response at energies that are lower than the bandgap energy without sacrificing the open-circuit voltage of the solar cell. These devices have been referred to as impurity photovoltaics (IPVs) [1] or intermediate band (IB) solar cells (IBSCs) [2]. IPV conventionally refers to the introduction of low-density Shockley–Read–Hall (SRH) centers in the forbidden bandgap, and minimal improvement in the short-circuit current is expected [1], [3], [4]. The utilization of energy states with highly radiative transitions is expected to dramatically increase the efficiency of IPV [5], where the concept is similar to that of IBSC.

The highly radiative electronic states may be introduced using impurities, dilute alloys, or quantum-confined structures. Since the original detailed balance 0-D model [2], further efforts have been published to enhance the understanding of this device, including the effect of intermediate level (IL) energy position and spectral overlap [6], [7], Auger generation [8], [9], thermodynamic consistency of subbandgap photovoltaics [10], quasi-drift-diffusion modeling [11], and equivalent circuit modeling [12]. Thus far, experimental data have not confirmed the high conversion efficiency expected for solar cells with subbandgap optical transitions, where both the open-circuit voltage $(V_{\rm oc})$ and the short-circuit current density $(J_{\rm sc})$ have been measured to be less than a single junction cell without ILs [13]–[15]. Existing 0-D detailed balance models do not provide adequate framework to explain this experimental behavior and also do not adequately incorporate physical processes for device design. The development of a 1-D drift-diffusion model would enable the design, optimization, and interpretation of subbandgap absorbing solar cells by incorporating material and device parameters, including generation–recombination, carrier transport, device dimensions, and doping profiles. Conventional drift-diffusion models for semiconductors only describe generation–recombination through nonradiative trap states [3], [4] and do not provide a straightforward means of incorporating radiative electron states corresponding to ILs. Furthermore, convergence for a conventional drift-diffusion numerical model becomes highly difficult when the concentration of intermediate states becomes larger than the background doping concentration of the host semiconductor material.

A quasi-drift-diffusion model has recently been presented [11], where the electron and hole continuity equations are solved for the device, without solving the Poisson equation. This model supports the proposed benefits for IBSC while partially incorporating drift and diffusion processes into a device model. The neglect of the Poisson equation in this model does not include the effect of space charge and the resulting influence on electrostatic potential. This model is therefore limited to the analysis of uniform regions of material and cannot properly analyze junction devices. This approach also has further limitations, including the inability to determine the filling of intermediate electron states and the assumption that diffusion current is dominant for charge collection.

In contrast to the quasi-drift-diffusion model, an IBSC model incorporating the Poisson equation and a modified SRH recombination process has been presented [13]. The Poisson equation is exclusively solved in the model in [13], while the electron and hole continuity equations are ignored with the assumption that electron and hole quasi-Fermi levels are flat in the base absorption region. For subbandgap absorbing solar cells, however, it is important to consider both the drift and diffusion current components, where junction solar cell devices will consist of both drift- and diffusion-dominated transport, depending on the

Manuscript received February 6, 2009; revised August 13, 2009. First published October 30, 2009; current version published November 20, 2009. This work was supported in part by the American Chemical Society Petroleum Research Fund. The review of this paper was arranged by Editor P. Panayotatos.

The authors are with the University of Michigan, Ann Arbor, MI 48109 USA (e-mail: shihchun@umich.edu).

Color versions of one or more of the figures in this paper are available online at http://ieeexplore.ieee.org.

Digital Object Identifier 10.1109/TED.2009.2032741

doping profiles and device geometry. Subbandgap absorbing solar cells will also typically desire thick absorber regions to maximize absorption via the ILs (absorption is typically weaker than band-to-band transitions), where absorption regions would not be fully depleted as assumed in many existing models.

In this paper, a 1-D drift-diffusion model is presented for solar cells with impurity levels using the self-consistent solution of the Poisson equation and continuity equations for electrons and holes. The radiative transitions via the ILs are modeled according to the original 0-D IBSC paper [2]. Radiative transitions associated with the ILs are generally not available in commercial and custom semiconductor drift-diffusion software packages. To date, the application of a drift-diffusion model has not been provided for IBSC with the exception of a quasi-1-D drift-diffusion model such as presented in [11] and [13]. The IPV/IBSC device model in this work is applied to determine the optimal device geometry and doping profile.

II. Model Description

The IL is modeled as a density of electron states (neutral when empty) at a singular energy within the bandgap. The IL states are assumed to be predominantly radiative since nonradiative transitions via the ILs would essentially preclude usage of such states in an effective subbandgap absorbing solar cell. Carrier loss mechanisms include radiative recombination via band-to-band and IL transitions, as well as nonradiative transitions via additional SRH centers. Transport between the ILs is ignored in this model since impurity states (such as N in III–N_x–V_{1-x} or O in II–O_x–VI_{1-x}) with density on the order of $N_I = 10^{18}$ cm^{-3} are not expected to significantly exhibit coupling. The value of N_I is chosen based on previous calculation on the optimal density of intermediate states [16]. Transport via the ILs relaxes the constraint that G–R balances locally, where the neglect of this effect provides a "worst case" estimate of the device performance. Nevertheless, it will become clear in Section IV that transport between ILs is not essential for optimized device structures.

The drift-diffusion model consists of the Poisson equation and continuity equation for electrons and holes. The Poisson equation for electrostatic potential (ψ) includes the charge density for electrons (n), holes (p), ionized acceptors (N_A^-), ionized donors (N_D^+), and charge in the intermediate states represented by the filling of the states (f) and the concentration of the intermediate states (N_I); ε_r is the relative permittivity, and ε_0 is the permittivity in vacuum. The continuity equations include the generation and recombination terms $G_{\rm if}$ and $R_{\rm if}$, where the subscripts denote the initial and final states in the valence band (VB), IL or IB, and conduction band (CB). Nonradiative generation–recombination is included in the term $R_{\rm nr}$. The details for the generation–recombination processes are described in the following:

$$\vec{\nabla}\cdot\varepsilon_r\varepsilon_0\,\vec{\nabla}\,\psi = -q\left(N_D^+ - N_A^- - n + p - fN_I\right) \tag{1a}$$

$$\vec{\nabla}\cdot\vec{J}_n = q(G_{\rm VC} + G_{\rm IC} - R_{\rm CV} - R_{\rm CI} - R_{\rm nr}) \tag{1b}$$

$$\vec{\nabla}\cdot\vec{J}_p = q(G_{\rm VC} + G_{\rm VI} - R_{\rm CV} - R_{\rm IV} - R_{\rm nr}). \tag{1c}$$

The electron and hole current equations include both the drift and diffusion components according to

$$J_n(x) = -qD_n\frac{dn}{dx} - q\mu_n nF \tag{2a}$$

$$J_p(x) = -qD_p\frac{dp}{dx} + q\mu_p pF \tag{2b}$$

where F is the electric field, D is the diffusion coefficient, and μ is the carrier mobility. State filling in the ILs is described by the Fermi–Dirac statistics [13]

$$f = \frac{1}{\exp(\frac{E_I - E_{\rm FI}}{kT}) + 1} \tag{3}$$

where E_I is the IL energy position and $E_{\rm FI}$ is the IL quasi-Fermi level.

The generation rates for optical transitions are defined by

$$G(x) = \int_{E_{\rm initial}}^{E_{\rm final}} I_s(E)\alpha e^{-\alpha_{\rm tot}x}\,dE \tag{4}$$

where E is the energy and α is the optical absorption coefficient for IL-to-CB, VB-to-IL, or VB-to-CB transitions. The total absorption coefficient is given by $\alpha_{\rm tot} = \alpha_{\rm IC} + \alpha_{\rm VI} + \alpha_{\rm VC}$. A fixed absorption coefficient is assumed for transitions via the IL. A truly accurate description would require dependence on the occupancy of the impurity states, although, in the case of fixed state filling, this effect is negligible. The calculations in this paper assume nonoverlapping absorption spectra for the intermediate and band-to-band transitions, where the effect of spectral overlap for IBSC has been studied elsewhere [6], [7]. The incident spectrum $I_s(E)$ is

$$I_s(E) = \frac{2\pi}{h^3c^2}\frac{Xf_sE^2}{\exp\left(\frac{E}{kT_s}\right) - 1} \tag{5}$$

where $f_s = 1/46\,050$ is the solid angle subtended by the sun, X is the solar concentration ($X = 1$ in this work), k is the Boltzmann constant, h is the Plank's constant, c is the speed of light, and $T_s = 5963$ K is the temperature of the sun.

Assuming nondegenerate conditions, the recombination rate for CB to VB can be written as

$$\begin{aligned} R_{\rm CV}(x) = {} & \frac{2\pi}{h^3c^2}\int_{E_G}^{\infty}\exp\left(\frac{-E}{kT}\right)\alpha_{\rm VC} \\ & \times\exp(-\alpha_{\rm tot}(x + W{\rm p}))\,E^2/n_i^2\,dE \\ & \times\left(n_i^2\exp\left(\frac{\mu_{\rm CV}}{kT}\right) - n_i^2\right) \\ = {} & B_r\left(np - n_i^2\right) \end{aligned} \tag{6}$$

where B_r is the radiative band-to-band recombination coefficient [11], $\mu_{\rm CV} = E_{\rm FC} - E_{\rm FV}$, $E_{\rm FC}$ and $E_{\rm FV}$ are the electron and hole quasi-Fermi levels, and n_i is the intrinsic carrier concentration. The nondegenerate approximation has been shown to be appropriate for 0-D modeling [17]. In our model, the nondegenerate approximation results in a maximum error of

$5.4 \times 10^{-7}\%$ in the Bose–Einstein factors used to calculate the recombination rates [2]. Similarly, the recombination rates for CB to IL and IL to VB are given by

$$R_{\mathrm{CI}}(x) = \frac{2\pi}{h^3c^2}\int_{E_L}^{E_H}\left(\frac{1}{\exp\left(\frac{E-\mu_{\mathrm{CI}}}{kT}\right)-1} - \frac{1}{\exp\left(\frac{E}{kT}\right)-1}\right) \times \alpha_{\mathrm{IC}}\exp^{-\alpha_{\mathrm{tot}}x}E^2\,dE \tag{7a}$$

$$R_{\mathrm{IV}}(x) = \frac{2\pi}{h^3c^2}\int_{E_H}^{E_G}\left(\frac{1}{\exp\left(\frac{E-\mu_{\mathrm{IV}}}{kT}\right)-1} - \frac{1}{\exp\left(\frac{E}{kT}\right)-1}\right) \times \alpha_{\mathrm{VI}}\exp^{-\alpha_{\mathrm{tot}}x}E^2\,dE. \tag{7b}$$

The aforementioned equations for R_{CI} and R_{IV} are dependent on $\mu_{\mathrm{CI}} = E_{\mathrm{FC}} - E_{\mathrm{FI}}$ and $\mu_{\mathrm{IV}} = E_{\mathrm{FI}} - E_{\mathrm{FV}}$, where mathematical transformations are used to write in terms of n and p. Equations (7a) and (7b) can be arranged into the following form [18]:

$$R_{\mathrm{CI}}(x) = R_{\mathrm{CI},0}\left[\exp\left(\frac{E_C - E_{\mathrm{FI}}}{kT}\right) \times n/N_c - 1\right] \tag{8a}$$

$$R_{\mathrm{IV}}(x) = R_{\mathrm{VI},0}\left[\exp\left(\frac{E_{\mathrm{FI}} - E_V}{kT}\right) \times p/N_V - 1\right] \tag{8b}$$

where E_C is the CB edge energy, E_V is the VB edge energy, and N_C and N_V are the electron and hole effective density of states. The relation between carrier concentration and quasi-Fermi levels is given by

$$n = N_C\exp\left(\frac{E_{\mathrm{FC}} - E_C}{kT}\right) \tag{9a}$$

$$p = N_V\exp\left(\frac{E_V - E_{\mathrm{FV}}}{kT}\right). \tag{9b}$$

Equations (9a) and (9b) provide more accurate expressions in comparison to the quasi-drift-diffusion model [11], where the quasi-Fermi level for the IL (E_{FI}) is assumed to be constant. The generation and recombination processes in the ILs are assumed to be balanced

$$R_{\mathrm{VI}}(E_{\mathrm{FI}},p,x) - G_{\mathrm{IV}}(x) = R_{\mathrm{CI}}(E_{\mathrm{FI}},n,x) - G_{\mathrm{IC}}(x) \tag{10}$$

implying that current flow via the IB is negligible [13].

SRH recombination is assumed to be the dominant nonradiative mechanism in a semiconductor, where the recombination rate is given by

$$R_{\mathrm{SRH}} = \frac{np - n_i^2}{\tau_p(n+n_1) + \tau_n(p+p_1)}$$

$$n_1 = n_i\exp\left(\frac{E_t - E_i}{kT}\right)$$

$$p_1 = n_i\exp\left(\frac{E_i - E_t}{kT}\right) \tag{11}$$

TABLE I
SIMULATION PARAMETERS

Band gap Energy E_{G}	1.95 eV
IL Energy position E_{I}	1.24 eV
Mobility μ_{n}, μ_{p}	100 cm^2/Vs
IL density of states N_{I}	10^{18} cm^{-3}
p-emitter, n-emitter doping N_A, N_D	10^{18} cm^{-3}
Effective density of states N_{C}, N_{V}	10^{19} cm^{-3}
Lattice temperature T	300 K
Solar temperature T_{s}	5963 K
Relative permittivity ε_{r}	10
p- and n- emitter width W_{p}, W_{n}	0.3 μm
Absorption coefficient α_{VC}, α_{IC}, α_{VI}	10^4 cm^{-1}

where n_i is the intrinsic carrier concentration, E_t is the trap energy position, and E_i is the intrinsic Fermi energy. In these simulations, the electron and hole lifetimes are assumed to be equal with the trap level at $E_t = E_i$, where SRH recombination is at a maximum. Other nonradiative recombination mechanisms can similarly be incorporated into (1b) and (1c) similar to conventional drift-diffusion models. Prior IBSC models generally did not include this capability since the continuity equations were solved in terms of μ_{CI} and μ_{IV}, rather than ψ, n, and p. The SRH recombination parameters are assumed to be uniform through the devices simulated in this paper, although the parameters could be assigned arbitrarily (e.g., higher density of trap states near interfaces or in the IL region).

Carrier concentration and electrostatic potential are calculated by solving the Poisson and continuity equations (1) using a coupled Newton's method. The solution under equilibrium is used as an initial guess. The boundary conditions assume ohmic contacts where the carrier concentrations are at the equilibrium values. The positions of E_{FC} and E_{FV} are calculated using (9a) and (9b). The parameters used for all the simulations are summarized in Table I. The bandgap energy and IL energy position are assigned the values of $E_G = 1.95$ eV and $E_I = 1.24$ eV, respectively, based on the optimal values obtained from the 0-D detailed balanced calculations [6], [18]. The device structure assumes a p- and n-type emitter with an IL absorber region, as shown in Fig. 1. The conversion efficiency of the solar cell is calculated by

$$\eta = \frac{J_{\mathrm{sc}} \times V_{\mathrm{oc}} \times FF}{P_{\mathrm{sun}}} \tag{12}$$

where J_{sc} is the short-circuit current density, V_{oc} is the open-circuit voltage, $FF = J_mV_m/J_{\mathrm{sc}}V_{\mathrm{oc}}$ is the fill factor, J_m and V_m are the current density and voltage at the operating point where the power output from the solar cell is maximum, respectively, and P_{sun} is the incident solar power density including concentration X [18].

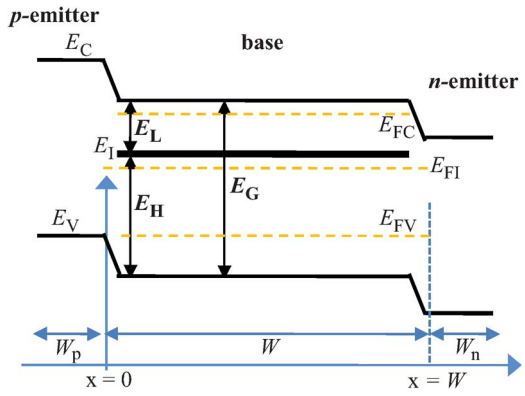

Fig. 1. Illustration of the prototype subbandgap absorbing solar cell device structure and energy band diagram.

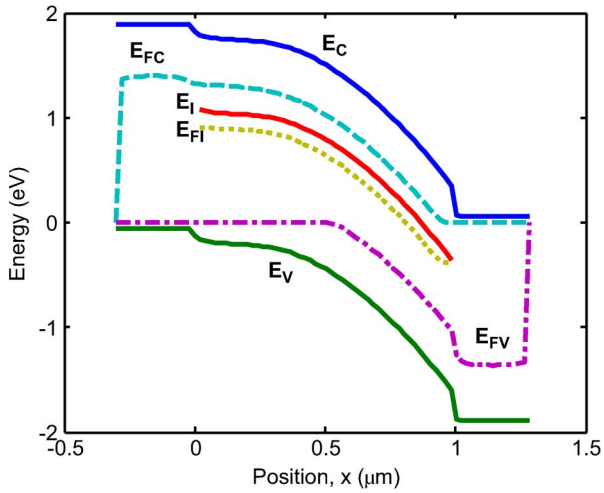

Fig. 2. Calculated energy band diagram for a lightly doped base at short circuit ($W = 1$ μm, N_D(base) $= 10^{14}$ cm^{-3}).

III. Lightly Doped Absorber

Initial simulations were conducted for a solar cell with uniform IL absorber layer with n-type doping of $N_D = 10^{14}$ cm^{-3} and width of $W = 1$ μm. The calculated band diagram for this device is shown in Fig. 2. The band diagram deviates from a conventional p-i-n (or similar p-π-n, p-υ-n) device, where the energy band profile variation is nearly linear in the $i\,(\pi, \upsilon)$ region. The nonlinear band profile is a result of the spatial variation of charge in the ILs and illustrates a primary shortcoming of 0-D models and quasi-1-D models, where linear potential profiles are assumed. The calculated quasi-Fermi level $E_{\rm FI}$ is significantly below E_I, with a corresponding low occupation of the IL. The assumption of a half-filled impurity states that [2], [11], and [17] will therefore not hold unless there is another mechanism for electron capture/escape such as field emission [18], [19]. Consequently, the high efficiency predicted by the 0-D models would not be realized in this device configuration.

The current-density–voltage (J–V) characteristics of this device under varying SRH lifetime are shown in Fig. 3. The finite slope near the short-circuit condition is due to an increase in the recombination rate with bias and reduced carrier collection due to the reduction in the electric field with increasing forward bias. The fill factor and resulting conversion efficiency (η) decrease with decreasing $\tau_{\rm SRH}$, as shown in the inset in Fig. 3. The decreased $V_{\rm oc}$ is the result of increased diode dark current due to nonradiative recombination. Thus far, experimental results have shown a decrease in $V_{\rm oc}$ for the case of IBSC, while the results for $J_{\rm sc}$ have been variable [12]–[15], [20], [21]. The results in Fig. 3 suggest that the reduction in $V_{\rm oc}$ may be associated with the increased SRH process associated with the material with impurity sites. In the extreme case of high SRH recombination, $J_{\rm sc}$ for IBSC may be reduced below the value of a control sample without IB.

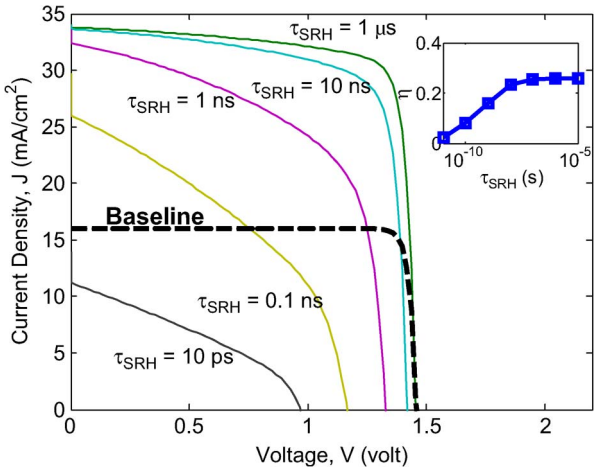

Fig. 3. Current-density–voltage characteristics for varying $\tau_{\rm SRH}$ and (inset) resulting conversion efficiency ($W = 1$ μm, N_D(base) $= 10^{14}$ cm^{-3}). The baseline is a p-i-n-type device without ILs and SRH.

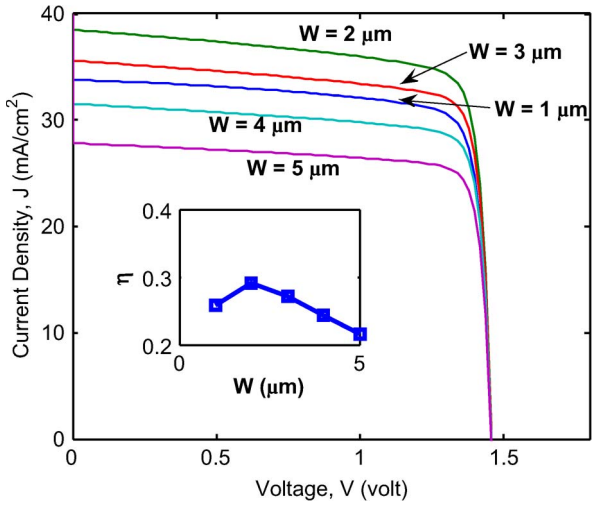

Fig. 4. Current-density–voltage characteristics for varying base width (no SRH recombination) and (inset) resulting conversion efficiency (N_D(base) $= 10^{14}$ cm^{-3}).

Solar cell conversion efficiency will depend on the base width (W), where there is a clear tradeoff related to maximizing optical absorption (large base width W) and maximizing carrier collection (small base width W). This tradeoff is typically deemed to be limited by SRH recombination. In these simulations, however, an optimal W is also found for the case of no SRH recombination. The J–V characteristics and conversion efficiency dependence on W for the case of no SRH are shown in Fig. 4. The decrease in efficiency for large W

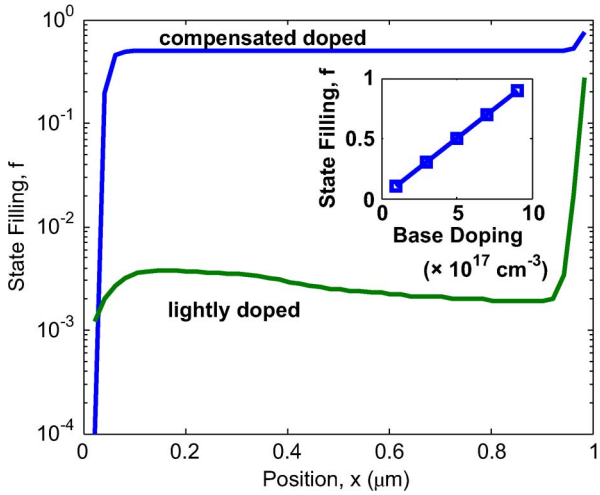

Fig. 5. Spatial dependence of state filling f for the case of $N_D = 5 \times 10^{17}$ cm^{-3} and $N_D = 10^{14}$ cm^{-3} and (inset) dependence on base doping.

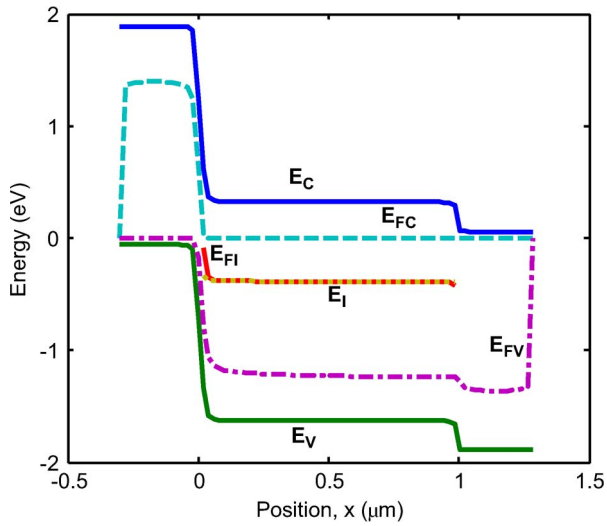

Fig. 6. Calculated energy band diagram for the case of compensated base doping with $W = 1$ μm, $N_I = 1 \times 10^{18}$ cm^{-3}, and $N_D = 5 \times 10^{17}$ cm^{-3} at short cirucit.

is the result of increased recombination rates via the ILs in the base region. The recombination processes via the IL will depend on the carrier populations in the IL, where increasing W will increase the filling of impurity states and increase the recombination rate. This result emphasizes the importance of the 1-D drift-diffusion model, where filling of impurity states and recombination rates have a significant dependence on the space charge characteristics of the device.

IV. Compensated Base Doping

One key outcome of the simulations for the devices with a uniformly doped absorber layer is the low carrier occupation in the ILs. It is desirable to increase the occupation of intermediate states to maximize photogeneration via these i states. However, increased carrier occupation in the intermediate states will significantly alter the space charge and potential profile. The achievement of the half-filled condition in the intermediate states throughout the full absorption region will therefore require a means of compensating the space charge. Varying the doping in the base absorber region is proposed in this paper to compensate the space charge that is related to carriers in the intermediate states.

The effect of absorber layer doping on IL occupation is shown in Fig. 5 for an impurity concentration of $N_I = 1 \times 10^{18}$ cm^{-3} and absorber doping varying between $N_D = 1 \times 10^{17}$ cm^{-3} and $N_D = 9 \times 10^{17}$ cm^{-3}. For a base doping that is half of N_I, the occupation of IL electron states is clamped at 50%. The resulting band diagram for the case of $N_I = 1 \times 10^{18}$ cm^{-3} and $N_D = 5 \times 10^{17}$ cm^{-3} is shown in Fig. 6. The compensated base doping approach results in a flatband region in the absorber, where the IL quasi-Fermi level ($E_{\rm FI}$) is pinned at E_I. With compensated base doping, the state filling is clamped at 50%. In this case, the band is flat, and the region is essentially charged neutral since the ionized dopant and IL space charge are nearly balanced. In this device design, the depletion region is limited to the region near the base/emitter junction. Carrier transport in the flatband region for this device would therefore be dominated by diffusion, rather than the drift current that would be typical for a p-i-n device structure.

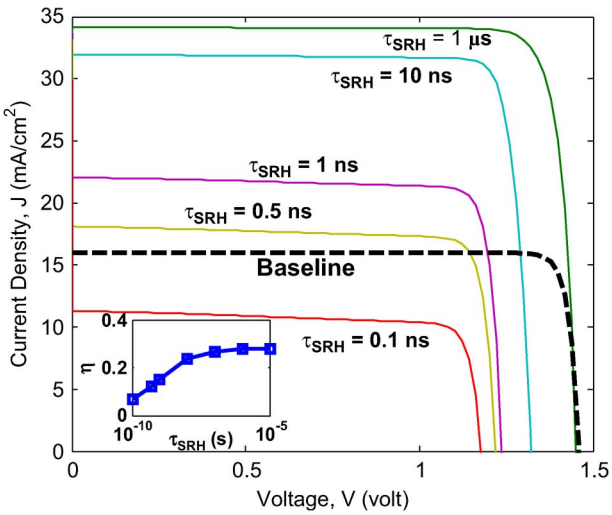

Fig. 7. Current-density–voltage characteristics for varying $\tau_{\rm SRH}$ and (inset) resulting conversion efficiency ($W = 1$ μm, N_D(base) $= 5 \times 10^{17}$ cm^{-3}). The baseline is a p-i-n-type device without ILs and SRH.

The original 0-D IBSC model [2] stated that the optimal conversion efficiency would require a half-filled IL and corresponding $E_{\rm FI}$ pinned at E_I. The original model also assumed that $E_{\rm FI}$, $E_{\rm FC}$, and $E_{\rm FV}$ are flat in the absorber base region. The proposed compensated base doping here provides a means of achieving these conditions, with a device structure that could provide the idealized maximum conversion efficiency. The compensated base doping approach, together with highly doped p- and n-emitters, maintains $V_{\rm OC}$ at a maximum value [18] and eliminates reduction in the fill factor due to the charge in ILs.

The J–V characteristics and conversion efficiency for varying SRH lifetime and base width are repeated for the case of compensated base doping (Figs. 7 and 8). An increase in

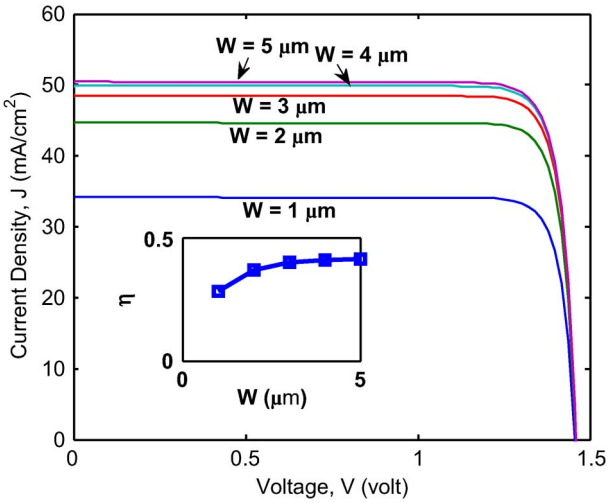

Fig. 8. Current-density–voltage characteristics for varying base width (no SRH recombination) and (inset) resulting conversion efficiency ($N_D(\text{base}) = 5 \times 10^{17}\ \text{cm}^{-3}$).

the conversion efficiency is calculated for the compensated base doping design in comparison to lightly doped absorber layers. The occupation of intermediate states is increased from nearly empty to $f \sim 0.5$ through compensated base doping. The resulting fill factor is improved from 0.811 to 0.871 ($W = 1\ \mu$m), and the maximum efficiency for large W is increased from 29.0% to 41.1%. The compensated base doping clamps the quasi-Fermi level E_{FI} at E_I regardless of the bias condition, preventing the depletion of the IL that would occur for the lightly doped base design. Similar to prior IBSC model formulations [6], [7], [11], [17], [19], the effect of IL occupation on the optical absorption coefficient is not incorporated in this model. The incorporation of IL occupation is expected to provide even lower efficiency values for the case of a lightly doped base, where low occupation in the impurity states would provide small values for absorption between the IL and CB (α_{IC}). The dependence of calculated efficiency on base width for the case of no SRH recombination in the compensated base doping design is shown in Fig. 8. The compensated base doping design eliminates any constraint on maximum W, in contrast to that in Fig. 4. The doping in this design serves to fix the occupation of the IL near $f = 0.5$, providing a fixed recombination rate that would otherwise vary with IL occupation due to space charge characteristics. The efficiency in Fig. 8 is $\eta = 28.05\%$ ($W = 1\ \mu$m) and 41.12% ($W = 5\ \mu$m), which is very close to the detailed balance limit of $\eta = 28.36\%$ ($W = 1\ \mu$m) and 44.57% ($W = 5\ \mu$m) [2]. This indicates that transport between impurity states is not essential for high-efficiency subbandgap absorbing solar cells once half-filled band and suppressed nonradiative recombination is achieved. One of the outcomes of the simulations for the compensated base doping scheme is an increase in the solar cell fill factor, where a more "boxlike" J–V curve is observed in relation to the lightly doped device structure. This result is consistent with recent experimental results, where a δ-doping scheme matched to the density of quantum dots has resulted in "boxlike" J–V curves [12]–[14]. On the contrary, IBSC consisting of quantum dots embedded in a p-i-n device structure has demonstrated reduced fill factors in comparison to baseline control samples [15], [21], which is similar to the case of a subbandgap absorbing solar cell with lightly doped base and increased SRH recombination presented in this paper.

V. Conclusion

A 1-D drift-diffusion modeling for IPVs has been presented. The results are consistent with prior 0-D models, verifying the ability to achieve high efficiency in the case of low nonradiative recombination and good electronic transport properties. The drift-diffusion model has identified that space charge effects are significant for subbandgap absorbing solar cells with lightly doped regions, where devices would have low occupation of IL and corresponding low conversion efficiencies. A doping compensation scheme is proposed to clamp the IL quasi-Fermi level at the IL position to reduce the space charge effects and to maximize optical generation. The compensated base doping scheme also eliminates the intrinsic dependence of efficiency on base doping due to space charge effects and increases the maximum achievable efficiency to $> 40\%$, near the values predicted for 0-D IBSC devices. The simulations are consistent with recent experimental demonstrations on quantum dot IBSC, suggesting that SRH can reduce V_{oc} and even J_{sc} below the baseline value. Moreover, the reduced fill factor in p-i-n structures is related to increased SRH recombination, while the increased fill factors for δ-doped structures are related to the achievement of the half-filled intermediate states. The 1-D drift-diffusion model facilitates the future design of subbandgap absorbing solar cells and related devices using the established framework of solving carrier continuity and electrostatic equations.

References

[1] M. Wolf, "Limitations and possibilities for improvement of photovoltaic solar energy converters," *Proc. IRE*, vol. 48, no. 7, pp. 1246–1263, Jul. 1960.

[2] A. Luque and A. Martí, "Increasing the efficiency of ideal solar cells by photon induced transitions at intermediate levels," *Phys. Rev. Lett.*, vol. 78, no. 26, pp. 5014–5017, Jun. 1997.

[3] M. Schmeits and A. A. Mani, "Impurity photovoltaic effect in c-Si solar cells. A numerical study," *J. Appl. Phys.*, vol. 85, no. 4, pp. 2207–2212, Feb. 1999.

[4] M. J. Keevers and M. A. Green, "Efficiency improvements of silicon solar cells by the impurity photovoltaic effect," *J. Appl. Phys.*, vol. 75, no. 8, pp. 4022–4031, Apr. 1994.

[5] A. S. Brown and M. A. Green, "Impurity photovoltaic effect: Fundamental energy conversion efficiency limit," *J. Appl. Phys.*, vol. 92, no. 3, pp. 1329–1336, Aug. 2002.

[6] T. S. Navruz and M. Saritas, "Efficiency variation of the intermediate band solar cell due to the overlap between absorption coefficients," *Sol. Energy Mater. Sol. Cells*, vol. 92, no. 3, pp. 273–282, 2008.

[7] L. Cuadra, A. Martí, and A. Luque, "Influence of the overlap between the absorption coefficients on the efficiency of the intermediate band solar cell," *IEEE Trans. Electron Devices*, vol. 51, no. 6, pp. 1002–1007, Jun. 2004.

[8] M. Leya, J. Boudaden, and Z. T. Kuznicki, "Thermodynamic efficiency of an intermediate band photovoltaic cell with low threshold Auger generation," *J. Appl. Phys.*, vol. 98, no. 4, pp. 044 905-1–044 905-5, Aug. 2005.

[9] A. Luque, A. Martí, and L. Cuadra, "Impact-ionization-assisted intermediate band solar cell," *IEEE Trans. Electron Devices*, vol. 50, no. 2, pp. 447–454, Feb. 2003.

[10] A. Luque, A. Martí, and L. Cuadra, "Thermodynamic consistency of sub-bandgap absorbing solar cell proposals," *IEEE Trans. Electron Devices*, vol. 48, no. 9, pp. 2118–2124, Sep. 2001.
[11] A. Martí, L. Cuadra, and A. Luque, "Quasi-drift diffusion model for the quantum dot intermediate band solar cell," *IEEE Trans. Electron Devices*, vol. 49, no. 9, p. 1632, Sep. 2002.
[12] A. Luque, A. Martí, C. Stanley, N. López, L. Cuadra, D. Zhou, J. L. Pearson, and A. McKee, "General equivalent circuit for intermediate band devices: Potentials, currents and electroluminescence," *J. Appl. Phys.*, vol. 96, no. 1, pp. 903–909, Jul. 2004.
[13] A. Luque, "Operation of the intermediate band solar cell under nonideal space charge region conditions and half filling of the intermediate band," *J. Appl. Phys.*, vol. 99, no. 9, p. 094 503, May 2006.
[14] A. Martí, N. López, E. Antolín, E. Canovas, A. Luque, C. R. Stanley, C. D. Farmer, and P. Diaz, "Emitter degradation in quantum dot intermediate band solar cells," *Appl. Phys. Lett.*, vol. 90, no. 23, p. 233 510, Jun. 2007.
[15] C. D. Cress, S. M. Hubbard, B. J. Landi, R. P. Raffaelle, and D. M. Wilt, "Quantum dot solar cell tolerance to alpha-particle irradiation," *Appl. Phys. Lett.*, vol. 91, no. 18, p. 183 108, Oct. 2007.
[16] A. S. Lin, W. Wang, and J. D. Phillips, "Model for intermediate band solar cells incorporating carrier transport and recombination and application to ZnTeO," *J. Appl. Phys.*, vol. 105, no. 6, p. 064 512, Mar. 2009.
[17] A. Luque and A. Martí, "A metallic intermediate band high efficiency solar cell," *Prog. Photovolt. Res. Appl.*, vol. 9, no. 2, pp. 73–86, Mar./Apr. 2001.
[18] G. Wei, K.-T. Shiu, N. C. Giebink, and S. R. Forrest, "Thermodynamic limits of quantum photovoltaic cell efficiency," *Appl. Phys. Lett.*, vol. 91, no. 22, p. 223 507, Nov. 2007.
[19] G. Wei and S. R. Forrest, "Intermediate-band solar cells employing quantum dots embedded in an energy fence barrier," *Nano Lett.*, vol. 7, no. 1, pp. 218–222, Jan. 2007.
[20] R. Oshima, A. Takata, and Y. Okada, "Strain-compensated InAs/GaNAs quantum dots for use in high-efficiency solar cells," *Appl. Phys. Lett.*, vol. 93, no. 8, p. 083 111, Aug. 2008.
[21] R. B. Laghumavarapu, A. Moscho, A. Khoshakhlagh, M. El-Emawy, L. F. Lester, and D. L. Huffaker, "GaSb/GaAs type II quantum dot solar cells for enhanced infrared spectral response," *Appl. Phys. Lett.*, vol. 90, no. 17, p. 173 125, Apr. 2007.

Albert S. Lin received the B.S. degree in electronic engineering from National Chiao Tung University, Hsinchu, Taiwan, in 2005 and the M.S. degree from the University of Michigan, Ann Arbor, in 2007, where he is currently working toward the Ph.D. degree in electrical engineering. The interest of his doctoral studies includes electromagnetic wave simulation and optical design of thin-film solar cell, modeling and theoretical study of intermediate band photovoltaics, and ZnTeO materials and devices.

Mr. Lin was the recipient of the Rackham Fellowship from the University of Michigan in 2005.

Jamie D. Phillips (M'01–SM'06) received the B.S., M.S., and Ph.D. degrees in electrical engineering from the University of Michigan, Ann Arbor, in 1994, 1996, and 1998, respectively. In his doctoral studies, he made key contributions to the epitaxial growth and device applications of self-assembled InGaAs/GaAs quantum dots, including quantum dot infrared photodetectors and quantum dot diode lasers.

From 1998 to 1999, he was a Postdoctoral Researcher with the Sandia National Laboratories, where he contributed to the growth of III–V antimonide materials for midinfrared lasers. From 1999 to 2001, he was a Research Scientist with the Rockwell Science Center, where he conducted research on HgCdTe infrared detectors. Since 2002, he has been a Member of the faculty with the Department of Electrical Engineering and Computer Science, University of Michigan, where he is currently an Associate Professor. His technical interests and contributions are in the growth, characterization, and device applications of compound semiconductor and oxide-based materials for optoelectronics and electronics, where he has published more than 70 peer-reviewed articles on these subjects.

Prof. Phillips is a member of the American Society for Engineering Education and the American Vacuum Society. He was the recipient of the NSF CAREER Award in 2003 and the DARPA MTO Young Faculty Award in 2007. He serves as a Guest Editor for the *Journal of Electronic Materials* special issue on wide bandgap materials.